IEEE Access
Multidisciplinary | Rapid Review | Open Access Journal

Received December 23, 2019, accepted January 2, 2020, date of publication January 6, 2020, date of current version January 15, 2020.

Digital Object Identifier 10.1109/ACCESS.2020.2964304

Genetic Algorithm Based Prototype Filter Design for Oriented Side Lobe Energy Suppression in FBMC System

JUNHUI ZHAO[1,2], (Senior Member, IEEE), SIYING LV[2], LIHUA YANG[2], AND SHANJIN NI[2]

[1]School of Information Engineering, East China Jiaotong University, Nanchang 330013, China
[2]School of Electronic and Information Engineering, Beijing Jiaotong University, Beijing 100044, China

Corresponding author: Junhui Zhao (junhuizhao@hotmail.com)

This work was supported in part by the National Natural Science Foundation of China under Grant 61661021 and Grant 61971191, in part by the Beijing Natural Science Foundation under Grant L182018, in part by the National Science and Technology Major Project of the Ministry of Science and Technology of China under Grant 2016ZX03001014-006, in part by the Open Research Fund of National Mobile Communications Research Laboratory, Southeast University under Grant 2017D14, and in part by the Jiangxi Provincial Cultivation Program for Academic and Technical Leaders of Major Subjects under Grant 20172BCB22016.

ABSTRACT The prototype filter design problem is investigated for the filter bank multicarrier (FBMC) system of the fifth generation (5G) physical-layer wireless communications. In order to further suppress the side lobe energy within a certain frequency range, different constraint factors need to be introduced to meet the various side lobe energy suppression demands. In this paper, we formulate a dual-objective optimization problem which minimizes the stopband energy with constrained factors and subjects to the ISI/ICI constraints. Considering the uncertain constrained factors, a suboptimization problem is proposed by constraining the total stopband energy and the side lobe energy of the first segment to minimize the side lobe energy of the second or the third segments. Then, the nested sequential quadratic program-genetic algorithm (NSGA), one of the artificial intelligence (AI) aided algorithms, is introduced to obtain the optimal solution of the dual-objective problem, in which the genetic algorithm (GA) is applied to acquire the optimal constrained factors and the sequential quadratic program (SQP) is applied to acquire the optimal filter coefficients. Numerical results validate that the proposed method can achieve orientated side lobe energy suppression at specified segments for satisfying different side lobe energy suppression requirements with the confirmed algorithm convergence.

INDEX TERMS Artificial intelligence (AI), filter bank multicarrier (FBMC), genetic algorithm (GA), oriented side lobe energy suppression, prototype filter design.

I. INTRODUCTION

In order to meet the exponential growth of data traffic, the upcoming fifth generation (5G) cellular communication has the potential to deliver the gigabit experience to mobile users [1], [2]. Multicarrier modulation (MCM) is an efficient technique for 5G physical-layer wireless communication systems due to its flexibility, low complexity, and high spectral efficiency [3], [4]. As one of the most critical representative MCM technologies, orthogonal frequency division multiplexing (OFDM) system has enjoyed its dominance for a long time in modern digital communications [5]. However, the OFDM system still has unsolved issues. More precisely, the insertion of cyclic prefixes (CPs) and the large side lobe in OFDM symbols result in a reduction of spectral efficiency, and the use of rectangular pulse shape on each subcarrier leads to high spectrum leakage and unreasonable degrees of freedom [6]. This paper shifts attention on the filter bank multicarrier (FBMC) system [7]. As an heir of the OFDM, the FBMC system does not require CPs, and it has the capability to achieve flexible exploitation of frequency. Moreover, compared with the OFDM system, it can bring advantages of lower side lobe energy, higher data transmission rate, and robustness to narrow-band interference [8]–[10].

The design of the prototype filter has been a core issue in the research of the FBMC techniques. The filter banks

The associate editor coordinating the review of this manuscript and approving it for publication was Guan Gui.

in FBMC are composed of synthesis filters and analysis filters, and both of them are originated from a spectrally well-designed prototype filter. The synthesis filters at the transmitter perform the multicarrier modulation, and the analysis filters is in charge of demodulation at the receiver. Instead of a fixed rectangular pulse shaping window, FBMC techniques use the well designed prototype-filter-based filter banks to channelize the broadband of signal. Optimizing various parameters of the waveform, the prototype filter can be obtained with a higher freedom degree [11]. Moreover, the spectrally well-designed prototype filter can improve the system performance [12], such as the stopband attenuation, side lobe energy suppression, inter-channel interference (ICI) and inter-symbol interference (ISI) [13]. The implementation of stopband energy minimization and side lobe energy suppression can effectively improve the spectral efficiency and frequency selectivity. Based on the improved frequency selectivity, data transmission as well as channel sensing can be carried out simultaneously. However, the ISI/ICI is at the expense of the increased stopband attenuation, and there is a tradeoff between the constraints of the ISI/ICI and the stopband attenuation. Thus, it is vital to design an excellent-quality prototype filter for FBMC system.

The prototype filter designing methods are classified into frequency sampling method, window function based method, and direct optimization method of filter coefficients. In the frequency sampling method and window function based method, the coefficients of the prototype filter are expressed as a closed-form mathematical formula with few adjustable structural parameters as variables. In contrast, by optimizing all coefficients, the direct optimization method has the potential to influence the filter performance, which is more likely to obtain a better-quality prototype filter than the other two design methods. Therefore, a few researches have been conducted on the direct optimization method of filter coefficients [11]. A constrained optimization model was constructed in the direct optimization method to minimize the stopband energy of the filter and satisfy the nearly perfect reconstruction (NPR) condition [14]–[16]. The established optimization model of the direct optimization method is usually highly nonlinear and nonconvex. As the number of subchannels increases, the gradient calculations increase due to the increased number of filter coefficients, which leads to a high computational complexity and the global optimum cannot be guaranteed in practice. The authors in [17] employed the α-based branch and bound (αBB) algorithm to reduce the unknown computational scale of the algorithm by constrained approximation. The designed prototype filter has lower stopband energy, however, the convergence time is difficult to accept in practice. Some modifications of the existing NPR filter were implemented in [18]. By setting the suitable thresholds to the newly added constraints of the redesigned optimization problem, the suboptimal filter coefficients could be obtained using the active set method. Though the designed prototype filter in [18] is able to provide better side lobe energy suppression and keep the NPR property, the employed active set method was easily influenced by the initial values and debased the quality of the optimal solution. However, in practical filter design applications, it is necessary to suppress the side lobe within specific frequency range while ensuring that the total stopband energy is kept at a low level. None of the above three proposed methods adds the constraint factors to achieve the oriented suppression of side lobe energy in FBMC system.

In this paper, we propose an artificial intelligence (AI) aided algorithm - the nested SQP-genetic algorithm (NSGA) to solve the oriented side lobe energy suppression issue in the design of FBMC filters, and the designed filters can achieve a better frequency localization and effectively improve spectral efficiency. The main contributions are summarized as follows:

- A novel constraint factors based dual-objective prototype filter optimization problem is formulated to further suppress the side lobe energy within certain frequency range, and thus achieving oriented side lobe energy suppression.
- Based on highly nonlinear and nonconvex characteristics of the proposed direct optimization problem of filter coefficients, we introduce the typical AI algorithm – genetic algorithm (GA) to obtain the best solution, which has the global searching capability without the assistance of specific areas.
- In order to optimize the three components of the constraint factor, and find out the relationship between each component and the constraint intensity of the corresponding side lobe segment, the NSGA is presented to acquire the optimal solution.
- Simulation results show that the designed filter not only achieves smaller stopband energy, but also effectively reduces the side lobe energy within specific frequency range.

The rest of this paper is organized as follows. In Section II, a typical FBMC system is described, in which the filter bank multicarrier with offset quadrature amplitude modulation (FBMC-OQAM) technique is utilized for subcarrier modulation and its derivation formula of ISI/ICI is given. In Section III, we develop the dual-objective optimization problem of the prototype filter design and introduce the constraint factor. The NSGA algorithm is proposed to get the optimal solution. The numerical results are given in Section IV. Finally, the conclusions are summarized in Section V.

II. FBMC SYSTEM MODEL WITH ISI/ICI

In this section, we introduce the FBMC-OQAM system [19], which has the capacity to achieve maximum spectrum utilization due to the overlapping property between adjacent subcarriers, and give the ISI/ICI derivation formulas of FBMC-OQAM system.

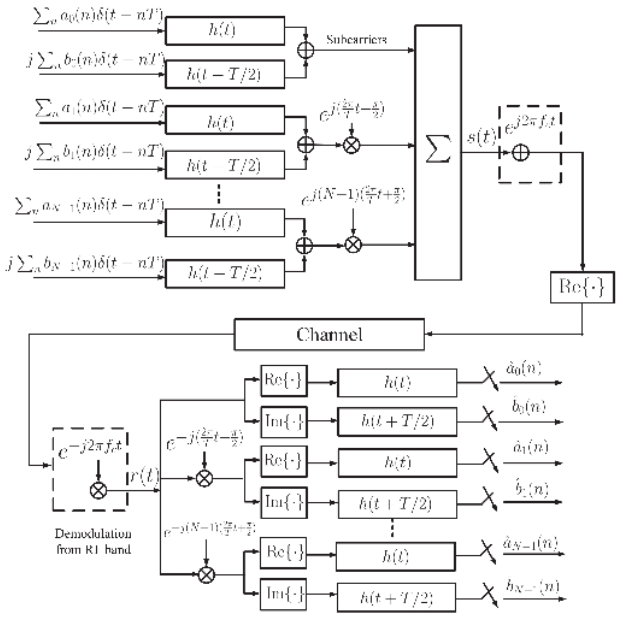

FIGURE 1. FBMC-OQAM system model.

A. FBMC-OQAM SYSTEM MODEL

Fig. 1 illustrates the FBMC-OQAM system model, which consists of a transmitter and a receiver. The input symbols at the transmitter can be expressed as

$$x_k(n) = a_k(n) + jb_k(n), \tag{1}$$

where the real and imaginary parts of the n^{th} symbol in the k^{th} subcarrier are $a_k(n)$ and $b_k(n)$, respectively. The components of in-phase and quadrature are staggered in time domain by $T/2$, where T is the symbol period. Then, the symbols go through a bank of transmission filters and are modulated using N subcarrier modulators whose carrier frequencies are $1/T$-spaced apart. The FBMC-OQAM modulated signals are represented as [20]

$$s(t) = \sum_{k=0}^{N-1} \sum_{n=-\infty}^{+\infty} [a_k(n)\, h(t - nT) + jb_k(n)\, h(t - nT - T/2)] e^{jk\varphi_t}, \tag{2}$$

where $h(t)$ is the impulse response of the prototype filter, and $\varphi_t = \frac{2\pi t}{T} + \frac{\pi}{2}$. After that, the signals are modulated to radio frequency (RF) band and transmitted as $s(t)$.

In an ideal transmission channel, the received signals $r(t)$ should be equal to the transmitted signals $s(t)$. After demodulated from RF band, the signals are passed to the N matched filters. The filtered signals are sampled with period T, and the output signals are presented as

$$\hat{x}_k(n) = \hat{a}_k(n) + j\hat{b}_k(n), \tag{3}$$

where $\hat{a}_k(n)$ and $\hat{b}_k(n)$ represent the real and imaginary parts of the n^{th} received symbol on k^{th} subchannel, respectively, and [21]

$$\hat{a}_k(n) = \sum_{n'=-\infty}^{\infty} \sum_{k'=0}^{N-1} \int_{-\infty}^{\infty} h(nT - t) \times \left\{ a_{k'}(n')\, h(t - n'T) \cos[(k' - k)\varphi_t] - b_{k'}(n') h(t - n'T - T/2) \sin[(k' - k)\varphi_t] \right\} dt, \tag{4}$$

and

$$\hat{b}_k(n) = \sum_{n'=-\infty}^{\infty} \sum_{k'=0}^{N-1} \int_{-\infty}^{\infty} h(nT - t + T/2) \times \left\{ a_{k'}(n')\, h(t - n'T) \sin[(k' - k)\varphi_t] - b_{k'}(n') h(t - n'T - T/2) \cos[(k' - k)\varphi_t] \right\} dt. \tag{5}$$

If the prototype filter satisfies the perfect reconstruction (PR) conditions [22], the output signals at the receiver equals the input signals at the transmitter, i.e.,

$$\hat{x}_k(n) = x_k(n). \tag{6}$$

Obviously, if the $h(t)$ is assumed to be real and even, the PR conditions are automatically satisfied [23].

B. THE FORMULA OF ISI/ICI IN FBMC-OQAM SYSTEM

The prototype filter should satisfy the PR conditions or provide NPR characteristics. However, the PR conditions are not indispensable because it is satisfied only in an ideal transmission system. Compared with the interferences caused by nonideal transmission channels, the interferences obtained from the NPR based filter banks are small enough. Moreover, the designed NPR properties based filter is more efficient, which can provide lower stopband energy than the designed PR based filter when they have the same filter length. Let $I^a_{k,n}$ and $I^b_{k,n}$ denote the interferences of ISI/ICI to $a_k(n)$ and $b_k(n)$, and their expected power are respectively represented as

$$\begin{aligned} &\text{Power}(I^a_{k,n}) \\ &= \mathbb{E}[(\hat{a}_k(n) - a_k(n))^2] \\ &= \mathbb{E}[(\sum_{n'=-\infty}^{\infty} \sum_{k'=0}^{N-1} \int_{-\infty}^{\infty} h(nT - t) \\ &\quad \times \{ a_{k'}(n')\, h(t - n'T) \cos[(k' - k)\varphi_t] \\ &\quad - b_{k'}(n') h(t - n'T - T/2) \sin[(k' - k)\varphi_t] \} dt - a_k(n))^2] \\ &= \mathbb{E}\left[\left(\sum_{n'=-\infty}^{\infty} \sum_{k'=0}^{N-1} I^a_{k,n,k',n'} - a_k(n) \right)^2 \right], \end{aligned} \tag{7}$$

and

$$\begin{aligned} \text{Power}(I^b_{k,n}) &= \mathbb{E}[(\hat{b}_k(n) - b_k(n))^2] \\ &= \mathbb{E}\left[\left(\sum_{n'=-\infty}^{\infty} \sum_{k'=0}^{N-1} I^b_{k,n,k',n'} - b_k(n) \right)^2 \right], \end{aligned} \tag{8}$$

where $I^a_{k,n,k',n'}$ denotes the contribution of $x_{k'}(n')$ to $\hat{a}_k(n)$ and $I^b_{k,n,k',n'}$ denotes the contribution of $x_{k'}(n')$ to $\hat{b}_k(n)$.

Then we have

$$I^a_{k,n,k',n'} = a_{k'}(n')C^1_{k,n,k'n'} - b_{k'}(n')C^2_{k,n,k',n'}, \tag{9}$$

where

$$C^1_{k,n,k',n'} = \int_{-\infty}^{\infty} h(nT-t)h(t-n'T)\cos[(k'-k)\varphi_t]dt, \tag{10}$$

$$C^2_{k,n,k',n'} = \int_{-\infty}^{\infty} h(nT-t)h\left(t-n'T-\frac{T}{2}\right)\sin[(k'-k)\varphi_t]dt. \tag{11}$$

We replace $h(t)$ with its discrete time version $h(l)$, $l = 0, 1, \ldots, L_p - 1$ for the purpose of designing the filter in the discrete time domain, where $h(l)$ corresponds to the filter impulse response at time lT/N, and L_p represents the discrete time filter length. Then equations (10) and (11) can be presented respectively as

$$C^1_{k,n,k',n'} = \sum_{l=0}^{L_p-1} h(nN-l)h(l-n'N) \times \cos[(k'-k)\left(\frac{2\pi l}{TN}+\frac{\pi}{2}\right)], \tag{12}$$

$$C^2_{k,n,k',n'} = \sum_{l=0}^{L_p-1} h(nN-l)h(l-n'N-\frac{N}{2}) \times \sin[(k'-k)\left(\frac{2\pi l}{TN}+\frac{\pi}{2}\right)]. \tag{13}$$

Because of the randomness of information bits, $a_{k'}(n')$ and $b_{k'}(n')$ are independent and symmetrical in the time-frequency domain with unit power, i.e.,

$$\mathbb{E}\left[a_{k'}(n')^2\right] = \mathbb{E}\left[b_{k'}(n')^2\right] = 1, \tag{14}$$

$$\mathbb{E}\left[a_{k'}(n')\right] = \mathbb{E}\left[b_{k'}(n')\right] = 0. \tag{15}$$

From (9), (14) and (15), we can obtain

$$\begin{aligned}&\mathbb{E}\left[(I^a_{k,n,k',n'})^2\right]\\ &= (C^1_{k,n,k',n'})^2\mathbb{E}\left[(a_{k'}(n'))^2\right] + (C^2_{k,n,k',n'})^2\mathbb{E}\left[(b_{k'}(n'))^2\right]\\ &\quad - 2C^1_{k,n,k',n'}C^2_{k,n,k',n'}\mathbb{E}\left[a_{k'}(n')\right]\mathbb{E}\left[b_{k'}(n')\right]\\ &= -2C^1_{k,n,k',n'}C^2_{k,n,k',n'}\mathbb{E}\left[a_{k'}(n')\right]\mathbb{E}\left[b_{k'}(n')\right].\end{aligned} \tag{16}$$

If $(k', n') = (k, n)$, we have

$$C^1_{k,n,k',n'} = \sum_{l=0}^{L_p-1} h(l)^2, \tag{17}$$

$$C^2_{k,n,k',n'} = 0. \tag{18}$$

Therefore,

$$I^a_{k,n,k,n} = a_k(n)\sum_{l=0}^{L_p-1} h(l)^2. \tag{19}$$

Apparently, it should be satisfied that

$$\sum_{l=0}^{L_p-1} h(l)^2 = 1, \tag{20}$$

$$I^a_{k,n,k,n} = a_k(n). \tag{21}$$

If $(k', n') \neq (k, n)$, we have

$$\begin{aligned}&\text{Power}(I^a_{k,n})\\ &= \mathbb{E}\left[\left(\sum_{n'=-\infty}^{\infty}\sum_{k'=0}^{N-1} I^a_{k,n,k',n'} - a_k(n)\right)^2\right]\\ &= \sum_{n'=-\infty}^{\infty}\left\{\sum_{k'=0,(k',n')\neq(k,n)}^{N-1}\mathbb{E}\left[(I^a_{k,n,k',n'})^2\right]\right\}\\ &\quad + \mathbb{E}\left[(I^a_{k,n,k,n} - a_k(n))^2\right]\\ &= \sum_{n'=-\infty}^{\infty}\left\{\sum_{k'=0,(k',n')\neq(k,n)}^{N-1}\mathbb{E}\left[\left(I^a_{k,n,k',n'}\right)^2\right]\right\}.\end{aligned} \tag{22}$$

If all the symbols are independent and identically distributed (i.i.d.) in time and frequency domain [17], Power$(I^a_{k,n})$ and Power$(I^b_{k,n})$ are independent of k, n. Then, the level of the entire system's ISI/ICI can be measured with any choice of k, n. Without loss of generality, we set $k' = n' = 0$. Under normal circumstances, the ISI/ICI energy of adjacent subcarriers and adjacent symbols is larger than that of non-adjacent subcarriers and non-adjacent symbols [23]. In order to simplify the calculation, we set $-1 \leq k \leq 1$, $-1 \leq n \leq 1$.

III. DIRECT OPTIMIZATION PROBLEM OF THE FILTER COEFFICIENTS

A. A DUAL-OBJECTIVE OPTIMIZATION METHODOLOGY

In this subsection, we formulate the direct optimization problem related to the design of filter coefficients. The transition between subchannels is located at the center of adjacent subcarriers when $\omega = \frac{2\pi}{N}$, which means that there is only a slight effect between adjacent subchannels. Moreover, we only consider the stopband region in the objective function. In order to limit the ISI/ICI energy, a lower threshold TH is introduced to control the error rate of the transmitted and received signals within a certain range for satisfying the design conditions of the NPR filter. Based on the obtained relationship of Power$(I^a_{k,n})$ = Power$(I^b_{k,n})$, we only consider one of the constraints. In this paper, we consider the ISI/ICI of real part in our optimization problem.

An even and real filter $h(l)$ with the length L_p is chosen that has the NPR characteristics, i.e.,

$$h(l) = h\left(L_p - 1 - l\right), \quad l = 0, 1, \ldots, L_p - 1. \tag{23}$$

The designed filter's Fourier transform is

$$H\left(e^{j\omega}\right) = \sum_{l=0}^{L_p-1} h(l)\, e^{-j\omega l}. \tag{24}$$

Then, the designed filter's magnitude response $h(l)$ is

$$\left|H\left(e^{j\omega}\right)\right| = \left|\sum_{l=0}^{L_p-1} h(l)\, e^{-j\omega l}\right|. \tag{25}$$

A classical optimization model of filter coefficients for FBMC is generally to minimize the stopband energy, and the optimization model is bounded by (20), (23), and the constraint of ISI/ICI. Then the corresponding optimization problem can be represented as **P1**:

$$\mathbf{P1}\quad \min_{\boldsymbol{h}} \int_{\omega_0}^{\pi} \left| \sum_{l=0}^{L_p-1} h(l)\, e^{-j\omega l} \right|^2 d\omega, \tag{26a}$$

$$\text{s.t. } h(l) = h\left(L_p - 1 - l\right), \tag{26b}$$

$$\text{Power}(I_{k,n}^{a}) < TH, \tag{26c}$$

$$\sum_{l=0}^{L_p-1} h(l)^2 = 1, \tag{26d}$$

where $\boldsymbol{h} = [h(0), h(1), \ldots, h\left(L_p - 1\right)]^T$.

Furthermore, according to (26b), only half of the variables are independent. Then we have

$$x = [x_1, x_2, \ldots, x_L] = \begin{cases} [h(0), h(1), \ldots, h(\frac{L_p}{2} - 1)]^T, & \text{if } L_p \text{ is even} \\ [h(0), h(1), \ldots, h(\frac{L_p - 1}{2})]^T, & \text{if } L_p \text{ is odd} \end{cases} \tag{27}$$

However, the classical model **P1** cannot suppress the side lobe within specific frequency range while ensuring that the total stopband energy is kept at a low level. Hence, we divide the stopband region represented as $[\frac{2\pi}{N}, \pi]$ into three segments where the energy of each segment is P_1, P_2, P_3, given as

$$\begin{aligned} P_1 &= \int_{\omega_0}^{2\omega_0} \left| H(e^{j\omega}) \right|^2 d\omega, \\ P_2 &= \int_{2\omega_0}^{3\omega_0} \left| H(e^{j\omega}) \right|^2 d\omega, \\ P_3 &= \int_{3\omega_0}^{\pi} \left| H(e^{j\omega}) \right|^2 d\omega. \end{aligned} \tag{28}$$

In order to achieve the oriented suppression of side lobe energy and reduce the side lobe leakage, we propose a dual-objective optimization model including two parts **P2-1** and **P2-2**:

The inter optimization problem **P2-1** is to minimize stopband energy under different constraint intensity, which is bounded by the equation (20), (23), and the constraint of ISI/ICI. The problem **P2-1** is formulated as

$$\mathbf{P2\text{-}1}:\quad \min_{\boldsymbol{h}} \left(\boldsymbol{\alpha}^T \cdot \boldsymbol{P}(\boldsymbol{h}) \right), \tag{29a}$$

$$\text{s.t. } h(l) = h\left(L_p - 1 - l\right), \tag{29b}$$

$$\text{Power}(I_{k,n}^{a}) < TH, \tag{29c}$$

$$\sum_{l=0}^{L_p-1} h(l)^2 = 1, \tag{29d}$$

where $\boldsymbol{\alpha} = [\alpha_1, \alpha_2, \alpha_3]^T$ is a vector with three constrained components, $\boldsymbol{h} = [h(0), h(1), \cdots, h\left(L_p - 1\right)]^T$, and $\boldsymbol{P}(\boldsymbol{h}) = [P_1, P_2, P_3]^T$ is side lobe energy.

It is known that different $\boldsymbol{\alpha}$ has different constraint intensity, the SQP algorithm is adopted to solve the optimization model **P2-1** with a known $\boldsymbol{\alpha}$. Then the corresponding $\boldsymbol{h}_{\boldsymbol{\alpha}}$ can be obtained through the SQP algorithm. Due to the fact that the first segment is close to passband boundary and the second/third segments are far from the passband boundary, we focus on minimizing the side lobe energy of the second/third segments under the constraint of total stopband energy and side lobe energy of the first segment. The outer optimization problem **P2-2** is represented as

$$\mathbf{P2\text{-}2}:\quad \min_{\boldsymbol{\alpha}}\ a \cdot P_2(\boldsymbol{h}_{\boldsymbol{\alpha}}) + b \cdot P_3(\boldsymbol{h}_{\boldsymbol{\alpha}}), \tag{30a}$$

$$\text{s.t. } \boldsymbol{h}_{\boldsymbol{\alpha}} = \text{SQP}(\boldsymbol{\alpha}), \tag{30b}$$

$$P_1(\boldsymbol{h}_{\boldsymbol{\alpha}}) \le Q_1, \tag{30c}$$

$$\sum_{i=1}^{3} P_i(\boldsymbol{h}_{\boldsymbol{\alpha}}) \le Q, \tag{30d}$$

where $\boldsymbol{h}_{\boldsymbol{\alpha}}$ can be obtained using the SQP algorithm with the input variable $\boldsymbol{\alpha}$, $a, b \in [0, 1]$ represent the options of two different optimization objectives, Q_1 and Q represent the constant constraint values of P_1 and P, respectively. Based on the above-obtained $\boldsymbol{h}_{\boldsymbol{\alpha}}$, the total stopband energy and the side lobe energy of each segment can be calculated. In order to optimize the constraint factor $\boldsymbol{\alpha}$ and find out the relationship between each component and the constraint intensity of corresponding side lobe segment, GA is proposed to solve the optimization problem **P2-2**.

Three different optimal objective functions P_2, P_3, and $P_2 + P_3$ can be chosen to optimize the constraint factor for oriented side lobe energy suppression. Due to the similar mathematical formulations between P_2 and P_3, for simplicity, we choose P_3 and $P_2 + P_3$ as the optimal objective functions in this paper. According to the objective functions P_3 and $P_2 + P_3$, the corresponding fitness functions can be established in GA.

B. THE NESTED SQP-GENETIC ALGORITHM

In this section, we propose the NSGA algorithm to solve the above dual-objective optimization problem. As we all known, the GA is one of the AI algorithms introduced by Holland [24], which is inspired by the biological evolution principle in nature with the help of the bio-inspired operators, known as selection, crossover and mutation [25], [26]. The GA-based optimization problem of prototype filter coefficients is described in detail below.

1) ENCODING

The population $\mathcal{N}$ consists of a certain number of individuals with encoded genes, these individuals represent the candidate solutions of the dual-objective optimization problem. The unique external manifestation (i.e., phenotype) of each individual is owed to the fact that its chromosome carries a certain feature, while the internal manifestation of the chromosome (i.e., genotype) is a combination of certain genes.

Therefore, we need to establish a mapping between phenotypes and genotypes through genetic encoding. Moreover, the operation of genetic operators is also based on the genetic level. In general, the most common encoding methods [26] for each individual in GA is to form a binary vector with a fixed length. Especially, based on the three constrained components, the binary vector of each NSGA individual is separated into three parts, and 12-bit binary encoding is applied for each part. The entire encoded population $\mathcal{N}$ can be denoted as

$$\mathcal{N} = [p_1, \cdots, p_i, \cdots, p_M], \tag{31}$$

where p_i is the 36-bit encoded vector of each NSGA individual, and M is the number of population $\mathcal{N}$.

2) FITNESS EVALUATION FUNCTION

Let fitness f_i denote the adaptability of each individual in a population [25], as the indicator of the evolutionary direction, the fitness f_i is the only part requiring the knowledge of our optimization model. In this paper, based on the objective functions P_3 and $P_2 + P_3$ in problem **P2-2**, the formulas for calculating NSGA individuals' *fitness* in a population are given as

$$\begin{aligned} f_{i,1} &= \frac{1}{P_{3,i}}, \\ f_{i,2} &= \frac{1}{P_{2,i} + P_{3,i}}, \end{aligned} \tag{32}$$

where $P_{2,i} = P_2(p_i)$ and $P_{3,i} = P_3(p_i)$. According to (32), the individual's fitness $f_{i,1}$ or $f_{i,2}$ is proportional to the adaptability of the individual, then the more promising individual will be selected in natural selection.

The maximal fitness of individuals in the $\mathcal{N}$ sequences is defined as

$$\begin{aligned} f_1^* &= \max_{1 \le i \le M} f_{i,1}, \\ f_2^* &= \max_{1 \le i \le M} f_{i,2}. \end{aligned} \tag{33}$$

3) MUTATION AND CROSSOVER OPERATION

Individuals in the population are crossed and mutated to produce the new offspring. For the sake of controlling the two evolutionary processes, the crossover and mutation are often under a certain probability [27], denoted as P_c and P_m. The traditional GA is inferior in the convergence speed and the quality of solution due to a fixed probability applied in crossover and mutation operators. In order to improve the convergence speed and optimization ability of the NSGA, the adaptive genetic operators [28] are applied, which may help to escape from the local optimum. The operators mean that if the population was trapped in the local optimum, the crossover and mutation probability should increase correspondingly, and if the solution space were too divergent, the crossover and mutation probability should decrease

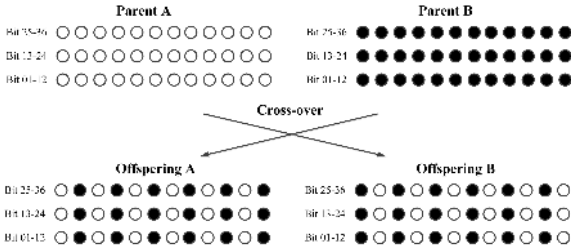

FIGURE 2. Illustration of crossover.

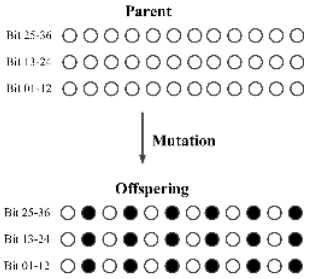

FIGURE 3. Illustration of mutation.

correspondingly. The expressions are given as

$$\begin{aligned} P_c &= \begin{cases} P_{c1} - \dfrac{(P_{c1} - P_{c2})(f - f_{\text{avg}})}{f_{\max} - f_{\text{avg}}}, & f > f_{\text{avg}} \\ P_{c1}, & f < f_{\text{avg}} \end{cases} \\ P_m &= \begin{cases} P_{m1} - \dfrac{(P_{m1} - P_{m2})(f - f_{\text{avg}})}{f_{\max} - f_{\text{avg}}}, & f > f_{\text{avg}} \\ P_{m1}, & f < f_{\text{avg}} \end{cases} \end{aligned} \tag{34}$$

where the upper and lower bounds of crossover probability are P_{c1} and P_{c2}, respectively, the upper and lower bounds of mutation probability are P_{m1} and P_{m2}, respectively. Maximal fitness value and average fitness value of individuals in a population are $f_{\max}$ and f_{avg}, respectively.

The illustration of crossover and mutation operations are depicted in Fig. 2 and Fig. 3. Taking the crossover process as an example, white and black balls represent genes belonging to parent A and parent B, respectively. Genes are separated from the two parents by randomly selecting odd points, and crossed-over by the adaptive genetic probability P_c to generate new descendants. The similar process can be adopted for the mutation (see Fig. 3).

4) SELECTION OPERATION

In order to avoid the elitists of the current population being omitted in the next generation, the *elitist selection* [29] and *roulette wheel selection* [30] are used in our selection process. According to the corresponding fitness functions, the individuals are sorted from the most-fit to the least-fit. Then the top S outstanding individuals (i.e., Elitists) are copied forcibly into the next generation, while the $M - S$ individuals should be chosen from all of individuals which include parents and their cross-mutated descendants using the *roulette wheel selection*. Thus, the total number of individuals remains constant, and the next new population is constructed.

TABLE 1. Parameters of NSGA.

Parameters	Value
Size of Population M	1000
Maximum Number of Iterations I	200
Upper Bound of Crossover Probability P_{c1}	0.8
Lower Bound of Crossover Probability P_{c2}	0.5
Upper Bound of Mutation Probability P_{m1}	0.3
Lower Bound of Mutation Probability P_{m2}	0.05
Number of Elitist Selection S	5
Repeated times of termination criterion K	20
Initial Value of SQP Algorithm h_s^0	0.977
Compared Maximal Fitness Deviation Δf	100
Number of Subcarriers N	64

5) TERMINATION CRITERION

The fitness values of all offspring are calculated by using (32), then the adaptability of all offspring are assessed. The evaluated maximal fitness of all offspring will replace the maximal counterpart of the previous generation if the current one is smaller than the previous one. The iteration is repeated until either the maximal fitness value keeps stable for successive generations or the maximal number of iterations is reached. Finally, the optimal solution is obtained.

The essence of GA is to solve unconstrained optimization problems. In order to ensure that the individuals belong to the feasible domain of **P2-2**, we need to repeatedly remove infeasible solutions from the current candidates after the crossover and mutation operations according to the inequality (30c) and (30d). The proposed NSGA algorithm can be summarized in Algorithm 1.

Algorithm 1 The Nested SQP-Genetic Search Algorithm

Step1. Initialize the value of SQP algorithm h_s^0, the population size M, the upper and lower bounds of crossover probability P_{c1} and P_{c2}, the upper and lower bounds of mutation probability P_{m1} and P_{m2}, the maximal number of iterations I, the repeated times of termination criterion K, the fitness threshold of termination criterion Δf, and the number of *elitist selection* S.

Step2. Randomly generate the initial population $\mathcal{N}^0$ of size M. Use the initial parent candidate individuals $\boldsymbol{\alpha}_i^0$ $(i = 1, \cdots, M)$ in $\mathcal{N}^0$ as the independent variables of SQP algorithm to solve the model **P2-1**. Obtain the filter coefficients $\boldsymbol{h}_{\boldsymbol{\alpha}_i^0}$ and the side lobe energy $P_1(\boldsymbol{h}_{\boldsymbol{\alpha}_i^0})$, $P_2(\boldsymbol{h}_{\boldsymbol{\alpha}_i^0})$, $P_3(\boldsymbol{h}_{\boldsymbol{\alpha}_i^0})$ and $P(\boldsymbol{h}_{\boldsymbol{\alpha}_i^0})$.

Step3. Crossover and mutate parent individuals using adaptive probabilities P_c and P_m to generate Z_1 and Z_2 new candidate offspring, respectively. Obtain their filter coefficients $\boldsymbol{h}_{\boldsymbol{\alpha}_i^l}$ and the side lobe energy $P_1(\boldsymbol{h}_{\boldsymbol{\alpha}_i^l})$, $P_2(\boldsymbol{h}_{\boldsymbol{\alpha}_i^l})$, $P_3(\boldsymbol{h}_{\boldsymbol{\alpha}_i^l})$ and $P(\boldsymbol{h}_{\boldsymbol{\alpha}_i^l})$ using the identical method as shown in Step 2.

Step4. Drop out all candidate individuals that do not belong to the feasible domain of **P2-2**. If the corresponding side lobe energy of some individuals cannot satisfy the constraint conditions (30c) and (30d) simultaneously, their fitness values are set as 0; Otherwise, go to the next step.

Step5. Calculate the fitness of all feasible individuals, and find out the maximal fitness of the parent feasible individuals $f^{l,*}$ in current population $\mathcal{N}^l$ according to the equation (32) and equation (33).

Step6. Combine *elitist selection* with *roulette wheel selection* to choose M new individuals from the feasible individuals of parent and offspring, then form the next generation population $\mathcal{N}^{l+1}$. Calculate the fitness of M new individuals and find out the individuals with maximal fitness $f^{l+1,*}$ as shown in Step 5.

Step7. Compare $f^{l+1,*}$ with $f^{l,*}$, if $\left|f^{l+1,*} - f^{l,*}\right| \leq \Delta f$ in successive K generations, or the times of iteration exceed the maximal number of iteration I, terminate the algorithm; Otherwise, go to Step 3.

IV. NUMERICAL SIMULATION AND ANALYSIS

In this section, the numerical simulation is conducted by the MATLAB (2014b) program running on a desktop computer equipped with an Intel i7-6700 3.4 GHz CPU to verify the effectiveness of the proposed method. Parameters of the NSGA algorithm are shown in TABLE 1.

Before we evaluate the performance advantage of the designed filters, we introduce three widely used filters listed below:

1) Optimized frequency sampling filters: the optimized frequency sampling filters denoted as $h_0(l)$ have the same objectives and constraints as those of **P1**. It is expressed as [11]

$$h_0(l) = P(0) + 2\sum_{i=1}^{W-1}(-1)P(i)\cos\left(\frac{2\pi i}{WN}(l+1)\right), \quad l = 0, 1, \cdots, WN-2, \tag{35}$$

where $P(i), i = 0, \cdots, W-1$ are adjustable filter coefficients. We replace $h_0(l)$ into the optimization problem **P1** and solve **P1** to obtain the optimized filter. For $L_p = 4N-1$, $W = 4$, then we can obtain $P(0) = 1$, $P(2) = \frac{\sqrt{2}}{2}$, $P(3) = \sqrt{1-P(1)^2}$. Therefore, there is only one parameter $P(1)$ that is needed to be optimized.

2) Optimized windowing based filters: the optimized windowing based filters denoted as $h_1(l)$ have the same objectives and constraints as those of **P1**. It is expressed as [31]

$$h_1(l) = w(l)h_c(l), \tag{36}$$

where $h_c(l)$ is the impulse response of an ideal causal lowpass filter expressed as

$$h_c(l) = \frac{\sin\left[w_c(l - L_p/2)\right]}{\pi(l - L_p/2)}, \quad l = 0, 1, \cdots, L_p - 1, \tag{37}$$

TABLE 2. Side lobe energy and constrained components of three segments with different Q and Q_1 threshold of h_3 and h_4.

Filter	Q_1	Q	P_1	P_2	P_3	P	α_1	α_2	α_3
$h_0(l)$	-	-	-64.56dB	-73.26dB	-69.45dB	-62.92dB	-	-	-
$h_1(l)$	-	-	-67.78dB	-80.82dB	-75.73dB	-66.95dB	-	-	-
$h_2(l)$	-	-	-58.72dB	-84.09dB	-94.27dB	-58.7dB	-	-	-
$h_3(l)$	-67dB	-65dB	-67.26dB	-99.13dB	-108.78dB	-67.26dB	0.12	10.62	69.56
		-70dB	-75.24dB	-100.58dB	-107.75dB	-75.23dB	0.37	10.57	72.14
		-75dB	-75.71dB	-101.19dB	-105.39dB	-75.69dB	0.78	27.73	89.6
		-80dB	-80.51dB	-91.36dB	-94.57dB	-80.01dB	15.80	25.95	92.07
	-72dB	-65dB	-74.82dB	-106.00dB	-106.56dB	-74.81dB	0.39	35.72	63.31
		-70dB	-74.00dB	-107.68dB	-108.59dB	-74.00dB	0.39	46.31	90.14
		-75dB	-75.35dB	-100.32dB	-107.59dB	-75.34dB	0.49	13.57	95.21
		-80dB	-81.26dB	-86.65dB	-94.40dB	-80.00dB	22.38	11.12	98.80
	-77dB	-65dB	-77.08dB	-98.51dB	-101.90dB	-77.04dB	1.83	35.55	99.19
		-70dB	-77.26dB	-88.59dB	-106.57dB	-76.94dB	0.88	0.88	87.57
		-75dB	-77.58dB	-93.09dB	-103.56dB	-77.45dB	0.90	2.76	62.55
		-80dB	-81.26dB	-86.65dB	-94.4dB	-80.00dB	22.38	11.12	98.80
$h_4(l)$	-67dB	-65dB	-74.73dB	-108.51dB	-105.60dB	-74.72dB	6.42	93.97	82.1
		-70dB	-73.94dB	-112.68dB	-107.18dB	-73.94dB	15.11	91.36	76.93
		-75dB	-75.82dB	-104.25dB	-103.06dB	-75.81dB	33.08	80.96	82.79
		-80dB	-80.39dB	-95.86dB	-92.64dB	-80.02dB	6.42	93.97	82.1
	-72dB	-65dB	-75.82dB	-104.25dB	-103.06dB	-75.81dB	6.01	69.07	81.96
		-70dB	-73.94dB	-112.68dB	-107.18dB	-73.94dB	11.79	70.61	56.84
		-75dB	-75.82dB	-104.25dB	-103.06dB	-75.81dB	26.05	55.64	70.12
		-80dB	-80.39dB	-95.85dB	-92.64dB	-80.02dB	26.05	55.64	70.12
	-77dB	-65dB	-77.00dB	-98.42dB	-102.29dB	-76.95dB	6.01	69.07	81.96
		-70dB	-77.00dB	-98.42dB	-102.29dB	-76.95dB	15.11	91.36	76.93
		-75dB	-77.00dB	-98.42dB	-102.29dB	-76.95dB	33.08	80.96	82.79
		-80dB	-80.39dB	-95.86dB	-92.64dB	-80.02dB	26.05	55.64	70.12

and $w(l)$ is the window function expressed as

$$w(l) = \sum_{i=0}^{3} (-1)^i A_i \cos\left(\frac{2\pi il}{L_p}\right). \tag{38}$$

The cut-off frequency w_c and the four weights factors A_i, $i = 0, 1, 2, 3$ are the parameters that are needed to be optimized for the optimized windowing based filters $h_1(l)$.

3) The PHYDYAS filter [32]: as one of the most typically frequency sampling technique based filter with the NPR property, the prototype filter of the PHYDYAS project denoted as $h_2(l)$ is also considered in our paper for comparison. The impulse response coefficients of $h_2(l)$ have a closed-form representation which can be given as

$$h_2(l) = 1 + 2\sum_{i=1}^{W-1} (-1)^i G_i \cos\left(\frac{2\pi i}{WN}(l+1)\right), \quad l = 0, 1, \cdots, WN-2, \tag{39}$$

where $W = 4$, $G_1 = 0.971960$, $G_2 = \frac{\sqrt{2}}{2}$ and $G_3 = 0.235147$ [33].

We design two filters with two different optimization objectives varied for different optimization constraints as follows:

- Minimize P_3 with different thresholds of Q_1 and Q constraints, we get filter $h_3(l)$, namely $a = 0, b = 1$.
- Minimize P_2 and P_3 with different thresholds of Q_1 and Q constraints, we get filter $h_4(l)$, namely $a = b = 1$.

In order to observe the influence of different Q and Q_1 values on the dual-objective optimization problem, we set a multi-group of Q and Q_1 for comparative analysis. TABLE 2 records the optimization results, which consist of the side lobe energy, stopband energy, and the acquired constrained components α_1, α_2 and α_3 with different thresholds, respectively. The optimization results illustrate that the normalized amplitude responses of two designed filters are definitely controlled by the predetermined constraints, and the two designed filters perform the better side lobe performances of the first segment. Moreover, the total stopband energy is lower than that of other three filters $h_0(l)-h_2(l)$. Without loss of generality, we take filter $h_3(l)$ and $h_4(l)$ with parameters $Q_1 = -70\text{dB}/Q = -75\text{dB}$ as examples for the following analysis.

TABLE 3 records the side lobe energy, the optimal constrained components α_1, α_2 and α_3 of three segments, and

TABLE 3. Side lobe energy and constraint factors of designed prototype filters h_3 and h_4.

Parameters	$h_0(l)$	$h_3(l)$	$h_4(l)$
Q(dB)	-	-75	-75
Q_1(dB)	-	-70	-70
P(dB)	-64.56	-75.7	-75.0
P_1(dB)	-73.26	-77.5	-75.0
P_2(dB)	-69.45	-80.4	-108.8
P_3(dB)	-62.92	-110.8	-104.3
α_1	-	0.64	0.46
α_2	-	0.07	80.20
α_3	-	97.29	53.03
$\alpha_1/(\alpha_1+\alpha_2+\alpha_3)$	-	0.65%	0.35%
$\alpha_2/(\alpha_1+\alpha_2+\alpha_3)$	-	0.07%	59.99%
$\alpha_3/(\alpha_1+\alpha_2+\alpha_3)$	-	99.28%	39.66%

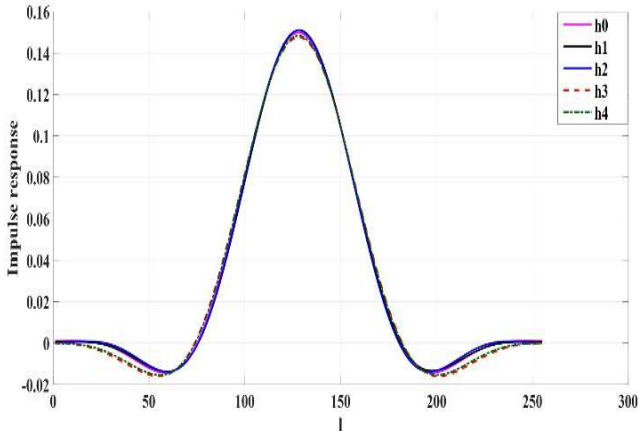

FIGURE 4. The impulse responses of $h_0(l)$, $h_1(l)$, $h_2(l)$, $h_3(l)$ and $h_4(l)$ with $Q_1 = -70\text{dB}/Q = -75\text{dB}$.

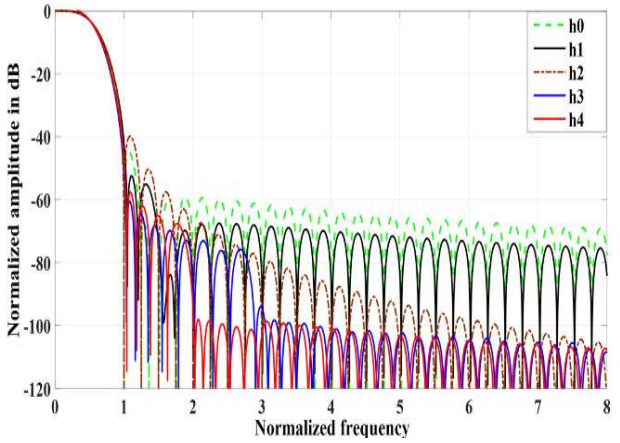

FIGURE 5. The normalized magnitude responses of $h_0(l)$, $h_1(l)$, $h_2(l)$, $h_3(l)$ and $h_4(l)$ with $Q_1 = -70\text{dB}/Q = -75\text{dB}$.

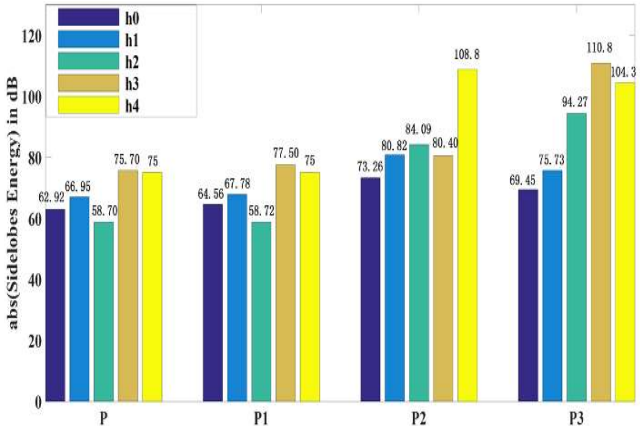

FIGURE 6. The side lobe energy of $h_0(l)$, $h_1(l)$, $h_2(l)$, $h_3(l)$ and $h_4(l)$ with $Q_1 = -70\text{dB}/Q = -75\text{dB}$.

the stopband energy of filter $h_3(l)$ and $h_4(l)$. The results depict that the side lobe energy of each frequency segment can be effectively suppressed due to the added constrained components. Moreover, the constrained components are in proportion to the binding intensity of the corresponding side lobe segment. These data confirm the availability of the proposed method.

Fig. 4 shows the impulse responses of filter $h_0(l) - h_4(l)$. Compared with the filters $h_0(l)$, $h_1(l)$ and $h_2(l)$, the impulse responses of the designed filter $h_3(l)$ and $h_4(l)$ with parameters $Q_1 = -70\text{dB}/Q = -75\text{dB}$ have similar trends with the other three filters for comparision in the passband. However, there is a noticeable improvement in stopband energy suppression of the proposed filters, which means that the designed two filters can effectively reduce the out-of-band energy leaks.

Fig. 5 illustrates the normalized magnitude responses of the filter $h_0(l) - h_4(l)$. Combined with the bar chart of Fig. 6, it is observed that the designed filter $h_3(l)$ and $h_4(l)$ can effectively suppress the side lobe energy of each segment and stopband energy, and both of the designed filters have a better performance than that of the filter $h_0(l)$, $h_1(l)$ and $h_2(l)$. The overall stopband energy of $h_3(l)$ and $h_4(l)$ are -75.7dB and -75.0dB, respectively, which are both significantly lower than the value of the $h_0(l)$, -62.9dB, by about 13dB and 12dB, respectively. The side lobe energy of the first segment of the designed filters $h_3(l)$ and $h_4(l)$ are -77.5dB and -75.0dB, respectively, which are also lower than the value of the $h_0(l)$, -64.6dB, by about 13dB and 10dB, respectively. Furthermore, $h_3(l)$ aiming to minimize P_3 has the lowest side lobe energy of the third segment, 110.8dB, and $h_4(l)$ aiming to minimize P_2 and P_3 has the best side lobe energy suppression performance of the second and third segment, 108.8dB and 104.3dB, respectively. As for optimized windowing based filter $h_1(l)$ and the PHYDYAS filter $h_2(l)$, the analytical results are similar to the filter $h_0(l)$ using optimized frequency sampling techniques. These simulation results verify that the proposed scheme achieves the oriented side lobe energy suppression in FBMC.

Fig. 7 plots the fitness curve corresponding to the optimal individual obtained from each iteration of the designed filter

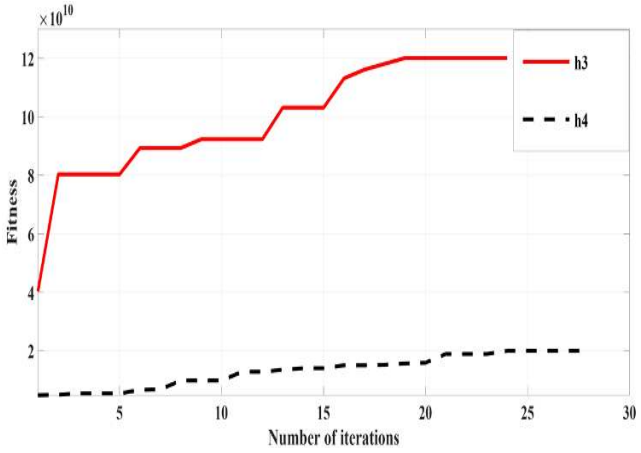

FIGURE 7. The fitness curves of $h_3(l)$ and $h_4(l)$ with $Q_1 = -70$dB/$Q = -75$dB corresponding to the optimal individual in each iteration.

TABLE 4. MSE between the transmitted symbols and the received symbols.

Parameters	Filters	MSE(real-part)	MSE(imag-part)
$TH = 10^{-4}$ $L_p = 4N-1$	$h_0(l)$	3.0443×10^{-5}	3.0375×10^{-5}
	$h_1(l)$	3.0495×10^{-5}	3.0260×10^{-5}
	$h_2(l)$	3.0332×10^{-5}	3.0375×10^{-5}
	$h_3(l)$	3.0260×10^{-5}	3.0182×10^{-5}
	$h_4(l)$	3.0294×10^{-5}	3.0416×10^{-5}

$h_3(l)$ and $h_4(l)$. It can be seen that the iterative processes corresponding to $h_3(l)$ and $h_4(l)$ tend to be stable in the 19^{th} and 24^{th} generations, respectively, and the proposed NSGA algorithm has an excellent algorithm convergence.

Simulation of the mean squared error (MSE) between the transmitted symbols and received symbols of the five filters $h_0(l) - h_4(l)$ are showed in Table 4. In order to verify the fact that the designed filters can perfectly satisfy the ISI/ICI requirements, we consider a pair of directly connected FBMC-OQAM transmitter and receiver with the designed filters under a Gaussian white noise channel, and the input signals before OQAM stagger are generated by 4-quadrature amplitude modulation (4-QAM), the MSE between the transmitted symbols and received symbols are then calculated. It can be seen that the designed filters $h_3(l)$ and $h_4(l)$ are both successfully constrained within the predefined $TH = 10^{-4}$, which can greatly satisfy the NPR property.

V. CONCLUSION

In this paper, we have proposed a novel approach for FBMC to design the filter coefficients directly, and the concept of constrained factors to further suppress the side lobe energy within certain frequency range has been introduced. In order to optimize filter coefficients directly, a dual-objective problem based on optimizing constrained factors has been formulated to minimize the side lobe energy of the second and the third segments, and constrain the total stopband energy as well as the side lobe energy of the first segment. A nested SQP-genetic algorithm has been applied to obtain the optimal solution, which performs better at the algorithm convergence. Numerical results have verified that the designed filters can achieve a better performance in oriented side lobe energy suppression at specified segments.

REFERENCES

[1] P. Banelli, S. Buzzi, G. Colavolpe, A. Modenini, F. Rusek, and A. Ugolini, "Modulation formats and waveforms for 5G networks: Who will be the heir of OFDM?: An overview of alternative modulation schemes for improved spectral efficiency," *IEEE Signal Process. Mag.*, vol. 31, no. 6, pp. 80–93, Nov. 2014.

[2] J. Zhao, S. Ni, L. Yang, Z. Zhang, Y. Gong, and X. You, "Multiband cooperation for 5G HetNets: A promising network paradigm," *IEEE Veh. Technol. Mag.*, vol. 14, no. 4, pp. 85–93, Dec. 2019.

[3] S. Ni, J. Zhao, H. H. Yang, and Y. Gong, "Enhancing downlink transmission in MIMO HetNet with wireless backhaul," *IEEE Trans. Veh. Technol.*, vol. 68, no. 7, pp. 6817–6832, Jul. 2019.

[4] C. He, L. Zhang, J. Mao, A. Cao, P. Xiao, and M. A. Imran, "Performance analysis and optimization of DCT-based multicarrier system on frequency-selective fading channels," *IEEE Access*, vol. 6, pp. 13075–13089, 2018.

[5] B. Farhang-Boroujeny, "Filter bank multicarrier modulation: A waveform candidate for 5G and beyond," *Adv. Elect. Eng.*, vol. 2014, Dec. 2014, Art. no. 482805.

[6] J. Zhao, S. Ni, and Y. Gong, "Peak-to-average power ratio reduction of FBMC/OQAM signal using a joint optimization scheme," *IEEE Access*, vol. 5, pp. 15810–15819, 2017.

[7] D. Qu, F. Wang, Y. Wang, T. Jiang, and B. Farhang-Boroujeny, "Improving spectral efficiency of FBMC-OQAM through virtual symbols," *IEEE Trans. Wireless Commun.*, vol. 16, no. 7, pp. 4204–4215, Jul. 2017.

[8] Z. Junhui, Y. Tao, G. Yi, W. Jiao, and F. Lei, "Power control algorithm of cognitive radio based on non-cooperative game theory," *China Commun.*, vol. 10, no. 11, pp. 143–154, Nov. 2013.

[9] B. Farhang-Boroujeny, "OFDM versus filter bank multicarrier," *IEEE Signal Process. Mag.*, vol. 28, no. 3, pp. 92–112, May 2011.

[10] S. Ni, J. Zhao, and Y. Gong, "Optimal pilot design in massive MIMO systems based on channel estimation," *IET Commun.*, vol. 11, no. 7, pp. 975–984, May 2017.

[11] A. Viholainen, T. Ihalainen, T. H. Stitz, M. Renfors, and M. Bellanger, "Prototype filter design for filter bank based multicarrier transmission," in *Proc. 17th Eur. Signal Process. Conf.*, Glasgow, U.K., Aug. 2009, pp. 1359–1363.

[12] J. Nadal, C. A. Nour, and A. Baghdadi, "Design and evaluation of a novel short prototype filter for FBMC/OQAM modulation," *IEEE Access*, vol. 6, pp. 19610–19625, 2018.

[13] I. V. L. Clarkson, "Orthogonal precoding for sidelobe suppression in DFT-based systems using block reflectors," in *Proc. IEEE Int. Conf. Acoust., Speech Signal Process. (ICASSP)*, New Orleans, LA, USA, Mar. 2017, pp. 3709–3713.

[14] J. Dou, Z. Zhang, J. Dang, L. Wu, Y. Wei, and C. Sun, "Properties and achievable data rate of a cyclic prefix based imperfect reconstruction filter bank multiple access system," *IET Commun.*, vol. 10, no. 17, pp. 2427–2434, Nov. 2016.

[15] S. Maeda, S. Nakao, and Y. Miyazato, "Three-dimensional fine structure of shock-containing free jets from supersonic square nozzles," in *Proc. AIAA Scitech Forum*, San Diego, CA, USA, Jan. 2019, p. 1606.

[16] W. Xu, Y. Li, J. Miao, J. Zhao, and X. Gao, "A novel design of sparse prototype filter for nearly perfect reconstruction cosine-modulated filter banks," *Algorithms*, vol. 11, no. 5, p. 77, May 2018.

[17] D. Chen, D. Qu, T. Jiang, and Y. He, "Prototype filter optimization to minimize stopband energy with NPR constraint for filter bank multicarrier modulation systems," *IEEE Trans. Signal Process.*, vol. 61, no. 1, pp. 159–169, Jan. 2013.

[18] D. Chen, D. Qu, and T. Jiang, "Novel prototype filter design for FBMC based cognitive radio systems through direct optimization of filter coefficients," in *Proc. Int. Conf. Wireless Commun. Signal Process (WCSP)*, Suzhou, China, Oct. 2010, pp. 1–6.

[19] D. Qu, S. Lu, and T. Jiang, "Multi-block joint optimization for the peak-to-average power ratio reduction of FBMC-OQAM signals," *IEEE Trans. Signal Process.*, vol. 61, no. 7, pp. 1605–1613, Apr. 2013.
[20] J. Kim, Y. Park, S. Weon, J. Jeong, S. Choi, and D. Hong, "A new filter-bank multicarrier system: The linearly processed FBMC system," *IEEE Trans. Wireless Commun.*, vol. 17, no. 7, pp. 4888–4898, Jul. 2018.
[21] F. Rottenberg, P. T. Dat, T.-H. Nguyen, A. Kanno, F. Horlin, J. Louveaux, and N. Yamamoto, "2×2 MIMO FBMC-OQAM signal transmission over a seamless fiber–wireless system in thew-band," *IEEE Photon. J.*, vol. 10, no. 2, Apr. 2018, Art. no. 7201814.
[22] M. Dominguezjimenez and N. Gonzalezprelcic, "Linear boundary extensions for finite length signals and paraunitary two-channel filterbanks," *IEEE Trans. Signal Process.*, vol. 52, no. 11, pp. 3213–3226, Nov. 2004.
[23] P. Amini, R. Kempter, and B. Farhang-Boroujeny, "A comparison of alternative filterbank multicarrier methods for cognitive radio systems," in *Proc. SDR Tech. Conf. Product Expo.*, Orlando, FL, USA, Nov. 2006.
[24] Y. Wang, W. Chen, and C. Tellambura, "Genetic algorithm based nearly optimal peak reduction tone set selection for adaptive amplitude clipping PAPR reduction," *IEEE Trans. Broadcast.*, vol. 58, no. 3, pp. 462–471, Sep. 2012.
[25] W. Song and C. Huang, "Mining high utility itemsets using bio-inspired algorithms: A diverse optimal value framework," *IEEE Access*, vol. 6, pp. 19568–19582, 2018.
[26] Y.-F. Cheng, W. Shao, S.-J. Zhang, and Y.-P. Li, "An improved multi-objective genetic algorithm for large planar array thinning," *IEEE Trans. Magn.*, vol. 52, no. 3, pp. 1–4, Mar. 2016.
[27] J. Zhao, X. Guan, and X. P. Li, "Power allocation based on genetic simulated annealing algorithm in cognitive radio networks," *Chin. J. Electron.*, vol. 22, no. 1, pp. 177–180, Jan. 2013.
[28] S. Pravesjit and K. Kantawong, "An improvement of genetic algorithm for optimization problem," in *Proc. IEEE Int. Conf. Digit. Arts (ICDAMT)*, Chiang Mai, Thailand, Mar. 2017, pp. 226–229.
[29] Y. Yang, J. Wu, J. Wang, and Z. Zhou, "An elitist multiobjective tabu search for optimal design of groundwater remediation systems," *Groundwater*, vol. 55, no. 6, pp. 811–826, Nov. 2017.
[30] W. Qian, J. Chai, Z. Xu, and Z. Zhang, "Differential evolution algorithm with multiple mutation strategies based on roulette wheel selection," *Appl. Intell.*, vol. 48, no. 10, pp. 3612–3629, Oct. 2018.
[31] P. Martín-Martín, R. Bregovic, A. Martín-Marcos, F. Cruz-Roldán, and T. Saramaki, "A generalized window approach for designing transmultiplexers," *IEEE Trans. Circuits Syst. I, Reg. Papers*, vol. 55, no. 9, pp. 2696–2706, Mar. 2008.
[32] H. Nam, M. Choi, C. Kim, D. Hong, and S. Choi, "A new filter-bank multicarrier system for QAM signal transmission and reception," in *Proc. IEEE Int. Conf. Commun. (ICC)*, Sydney, NSW, Australia, Jun. 2014.
[33] M. G. Bellanger, "Specification and design of a prototype filter for filter bank based multicarrier transmission," in *Proc. IEEE Int. Conf. Acoust., Speech Signal Process.*, Salt Lake City, UT, USA, May 2001, pp. 2417–2420.

JUNHUI ZHAO (Senior Member, IEEE) received the M.S. and Ph.D. degrees from Southeast University, Nanjing, China, in 1998 and 2004, respectively. From 1998 to 1999, he was with the Nanjing Institute of Engineers, ZTE Corporation. Then, he was an Assistant Professor with the Faculty of Information Technology, in 2004, and the Macao University of Science and Technology, and continued there till 2007 as an Associate Professor. Meanwhile, he was also a short term Visiting Scholar with Yonsei University, South Korea, in 2004, and a Visiting Scholar with Nanyang Technological University, Singapore, from 2013 to 2014. In 2008, he joined Beijing Jiaotong University as an Associate Professor. Since 2016, he has been with the School of Information Engineering, East China Jiaotong University. He is currently a Professor with the School of Electronics and Information Engineering, Beijing Jiaotong University. His current research interests include wireless and mobile communications and the related applications, which contain 5G mobile communication technology, high-speed railway communications, vehicle communication networks, wireless localization, and cognitive radio.

SIYING LV received the B.Eng. degree in information and computing science from Beijing Jiaotong University, Beijing, China, in 2017, where she is currently pursuing the M.S. degree. Her research interest includes 5G physical layer.

LIHUA YANG is currently pursuing the Ph.D. degree with the School of Electronic and Information Engineering, Beijing Jiaotong University. Her work focuses on the modeling and analysis of millimeter-wave networks, 5G HetNets, and the exploitation of interference management for ultradense networks. Her research interests include HetNets, ultradense networks, control/plane split architecture, interference management, stochastic geometry, and convex optimization.

SHANJIN NI received the B.Eng. degree in communication engineering from the China University of Geosciences, Wuhan, China, in 2014. He is currently pursuing the Ph.D. degree with Beijing Jiaotong University, Beijing. His research interests include massive MIMO communications, deep learning, and optimization techniques.